Proceedings of ISFOG 2025
5TH INTERNATIONAL SYMPOSIUM ON
FRONTIERS IN OFFSHORE GEOTECHNICS
Nantes, France | June 9-13 2025

ISBN 978-2-85782-758-0

Numerical investigation of multidirectional response of shared anchor piles for offshore wind

A. Rashidi Mehrabadi*
University of Southampton, Southampton, United Kingdom

B. Cerfontaine, S. Gourvenec, D.J. White
University of Southampton, Southampton, United Kingdom
* *A.Rashidimehrabadi@soton.ac.uk*

ABSTRACT: Shared anchor systems, where multiple FOWTs are connected to a single anchor, can reduce the number of anchors across a windfarm by up to 60%, hence reduce the overall cost of energy and demands on the supply chain. During a single storm episode, the resultant anchor load acts predominantly in the direction of prevailing wind, wave, and currents, but over a design lifetime, loads may act in different principal directions. Multidirectional cyclic loading may accelerate vertical ratcheting and degrade the holding resistance of an anchor. However, this behaviour is currently poorly understood. This paper presents results of a numerical study investigating the drained cyclic response of shared pile anchors under multidirectional one-way cyclic loads. Finite element simulations of a wished-in-place pile in sand are modelled using the hypoplastic constitutive model. Inclined loading relative to the seabed, representative of a taut configuration, is considered, in conjunction with the impact of load directionality from two consecutive storms, covering a range of load path directions. The results of the multidirectional tests reveal an increase of cyclic displacement accumulation compared to the unidirectional case. A factor to describe this amplification from multidirectionality is proposed based on the findings, to quantify pile uplift ratcheting as a function of the multidirectional load attributes.

Keywords: Anchors; Shared anchors; Floating Offshore Wind; Cyclic loading

1 INTRODUCTION

In the UK alone, projections indicate that between now and 2050, thousands of anchors will need to be installed annually to secure floating wind turbines and achieve carbon neutrality (Cerfontaine et al., 2023). This substantial demand challenges the current supply chain and may impact net zero targets. Shared anchors, or multiline anchors, have emerged as an innovative solution, allowing multiple mooring lines to connect to a single anchor, potentially reducing anchor needs by up to 60% and helping to lower the overall cost of energy. This approach has already been used on the Hywind Tampen offshore wind project (Equinor, 2023). Shared anchors offer the potential to lower peak lateral loads during storms as opposing mooring line orientations balance the forces (Fontana et al., 2018; Pillai et al., 2022).

Shared anchors experience complex cyclic loading over time. Firstly, the resulting net force is more inclined to the vertical than the individual mooring forces, as while horizontal components can offset each other, vertical components accumulate. This effect is especially notable in taut (or semi-taut) mooring configurations, which help minimize the mooring system's footprint and mass of raw material required compared to traditional catenary moorings. Secondly, while anchor loads are generally aligned with a predominant wind, wave, current (WWC) direction during a single storm, loading of sequential storms may vary over the design life of the wind turbine (Fontana et al., 2018; Pillai et al., 2022). This multidirectional cyclic loading can lead to vertical ratcheting of an anchor, degrading the capacity.

In an experimental investigation, Herduin (2019) studied the response of shared pile anchors under multidirectional cyclic loading for an array of wave energy converters. While this study provides an understanding of multidirectional anchor behavior, the load patterns applied do not align with those for offshore wind anchors, based on aero-hydrodynamical studies of wind turbine systems.

This study explores the effect of the multidirectional loading caused by successive storms, where each storm is represented by a one-way load pattern, composed of 10 cycles, representing the equivalent number of cycles, $N_{eq,}$ of the peak event. The effect of the extent of multidirectionality between storms is explored through 5 simulations in which a first packet of storm loading is applied in one direction, followed by a second packet of loading applied in another direction – varying from 0° to 180° between simulations. This method enables an analysis of how directional changes between storm events influences accumulated pile displacement.

2 FINITE ELEMENT MODEL

A 3D numerical model of a shared pile anchor was simulated in the finite element software ABAQUS (Dassault Systèmes, 2023) and subjected to two consecutive idealised storms with varying predominant load directions.

2.1 Numerical Model

A short open-ended rigid pile with diameter (D) of 2.3 meters, embedded length (L) of 15.5 meters and thickness (t) of 0.03 m was modelled for the offshore anchor. The model pile is assumed wished in place. The soil domain was modelled as a cylinder with diameter of 18D (41.5 m) and depth of 1.5L (23.2 m), which was shown to be sufficiently remote to have no effect on the pile response. To prevent soil overtopping the pile under large deformations, an additional stickup length of 1.5 m was modelled. The load reference point (LRP) is taken at mudline, not at the top of the stickup. The model was discretized using 8-noded linear, reduced integration brick elements (C3D8R). The FE mesh is more refined close to the anchor pile in areas of large stress concentration. A mesh composed of 23,858 elements was selected, as it did not exhibit any difference in load-displacement relationship when compared to a denser mesh of 89,501 elements. An illustration of the finite element mesh used for this study is shown in Figure 1.

2.2 Constitutive model

The hypoplastic model (Niemunis and Herle, 1997) with intergranular strain is used to capture the cyclic behaviour of the sand material. Fine silica sand parameters (Chow et al., 2019) were adopted in a user defined material code for hypoplasticity (Staubach et al., 2021). The soil was modelled as homogeneous, and dense at 75% relative density. At such relative density, the permeability reported for the sand is 3.13 $\times$ 10^{-5} m/s (Chow et al., 2019). A nominal cohesion of 3 kPa was adopted to facilitate numerical convergence in low stress elements (e.g. Sheil and McCabe (2017)).

The pile-soil interface was modelled by zero-thickness interface elements. For the tangential behaviour, a penalty approach was used with a friction coefficient of 0.2 to represent a near-smooth interface for the pile. Hard contact was selected for the normal behaviour and the penalty stiffness was reduced by a factor of 100 compared to the soil stiffness to enhance convergence with no effect on monotonic response and minimal effect on cyclic response.

The anchor pile was modelled as linear elastic and properties were assigned for an effectively rigid pile response (E = 68 GPa, ν = 0.36), being much stiffer than the surrounding soil. A section of the anchor at the mudline level was assigned as a rigid body to enable applying a point load or displacement at the centre of the pile at the mudline elevation with no eccentricity.

2.3 Testing Program

The padeye position, i.e. the application point for the net force from attached mooring lines, and the location of pile displacement measurement, was defined as the axis of the pile at mudline level. The load was applied at 45° to the horizontal mudline plane, to represent the resultant load of a shared taut mooring system whose lines are inclined between 5 to 25° to the mudline (Coughlan, 2024). Pile movement during a storm is dominated by the large load events (Richards et al. (2020), such that the effect of a storm, can be practically represented by a time series simulating only the peak loads. In this study, each storm was represented by a packet of loading of 10 cycles of constant amplitude (consistent with Fontana et al. (2018)). A first packet was applied as one-way cyclic loading in the vertical plane of the x-direction (Figure 1). The direction of the second packet, composed of 10 one-way cycles of the same amplitude, made an angle α in the horizontal plane with the x-direction. The sand response is assumed to be drained under typical wave loading, such that the frequency of applied loading is arbitrary.

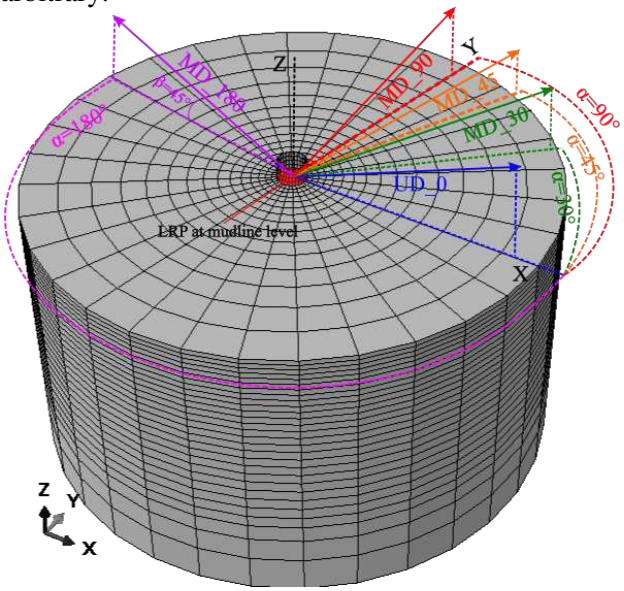

Figure 1 Finite element mesh coordinate system and illustration of the testing program. Loading reference point (LRP) shown at mudline level.

The test program is illustrated graphically in Figure 1. An initial monotonic test determined the anchor ultimate limit state. The unidirectional (UD) test is the simulation where there is no change of direction between the successive packets of storm loading. The four multidirectional tests (MD) explore the effect of a change in storm direction in the horizontal plane.

The magnitude and symmetry of the cyclic load is given by the nondimensional parameters ζ_b and ζ_c (LeBlanc et al. (2010)).

$$\zeta_b = \frac{F_{max}}{F_{ult,45}} = 0.95$$

$$\zeta_c = \frac{F_{min}}{F_{max}} = 0.5$$

The ultimate capacity, $F_{ult,45}$ is the load at which a plateau was achieved in the force-controlled load-displacement response under 45° inclination to the horizontal. The forces F_{max} and F_{min} represent the maximum and minimum cyclic load magnitudes. These values were selected to simulate severe storm loads with a minimum number of cycles for computational efficiency.

Figure 2 illustrates the two packets of cyclic loading applied to the pile. The first storm packet of 10 cycles is highlighted by the blue bracket with Point A marking the end of this loading phase. Following this, a brief unloading phase in the first loading direction occurs with Point B marking the end of this unloading stage. This point represents the initial condition at which the second storm begins.

The second storm packet of a further 10 cycles (purple bracket) begins immediately after Point B and continues until the end of the analysis. Point C denotes the end of this second packet of cyclic loading. The brief unloading and reloading transition between the storms was implemented to replicate reality, where sequential storms would be interspered with a period of calm weather, and also to facilitate the convergence of the numerical simulations, as any abrupt discontinuity in load can lead to convergence issues in the model, usually driven by changes of contact areas along the interface.

This segmented loading protocol, with Points A, B, and C marking key transitions, are used in subsequent analysis of the pile response.

3 RESULTS

3.1 Typical monotonic and cyclic load-displacement responses

The load-displacement response at the load reference point under monotonic and cyclic loading is shown in Figure 3 for the case of no change in direction of loading between storm packets (UD). The ultimate capacity, $F_{ult,45}$ = 4555 kN, was obtained when the load reached its peak and stabilized under monotonic loading. Key points in the simulation, defined in Figure 2 are marked on Figure 3.

Figure 4 illustrates the load-displacement response of the pile under cyclic loading during the second storm phase for the case where the load angle varies by 90° compared to the initial storm (i.e. MD_90). The horizontal load-displacement response (Figure 4a) shows the typical closed-loop pattern of cyclic loading, with minimal displacement accumulation over each cycle (on average 1 mm/cycle). This behaviour suggests that, in the horizontal direction, displacement accumulation remains limited and does not significantly increase under cyclic loading conditions. In contrast, Figure 4b highlights a more substantial accumulation of vertical displacement with each loading cycle (on average 10 mm/cycle). Although the trend of vertical displacement accumulation reduces with each cycle, such vertical displacement accumulation could have implications for pile stability, as the ongoing vertical uplift under cyclic loading reduces the pile-soil contact area, hence the vertical capacity.

3.2 Effect of storm directionality on the load-displacement response.

The normalized resultant displacement (d_r/D) with cycles across the different test configurations is illustrated in Figure 5, providing insight into the effect of variation in storm directions on pile displacement accumulation. The normalized resultant displacement (d_r) is $d_r = \sqrt{d_h^2 + d_v^2}$, where d_h is the anchor horizontal displacement and d_v is the anchor vertical displacement. Also, $d_h = \sqrt{d_x^2 + d_y^2}$, where d_x and d_y are anchor displacement in the x and y directions, respectively. The accumulation of displacement for the first 10 cycles is the same for all configurations (as would be expected), but the displacement accumulation rate diverges during the second storm depending on the change in load direction. Smaller directional deviations (MD_30 at 30° and MD_45 at 45°) show a rate of displacement similar to the unidirectional test (UD_0).

In contrast, larger changes in load directionality between storms (MD_90 at 90° and MD_180 at 180°) lead to more significant pile displacement accumulation, underscoring the impact of substantial load direction changes on long-term pile displacement behaviour.

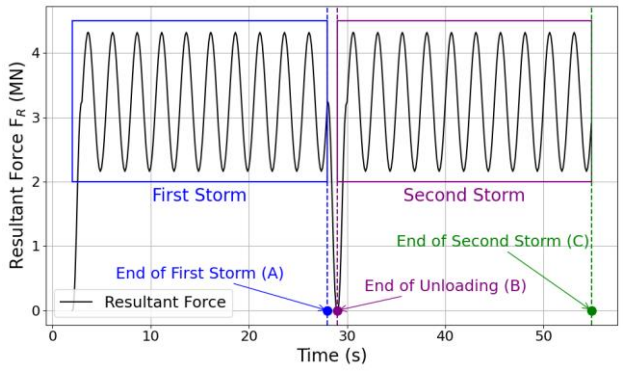

Figure 2 Resultant force time history in unidirectional test.

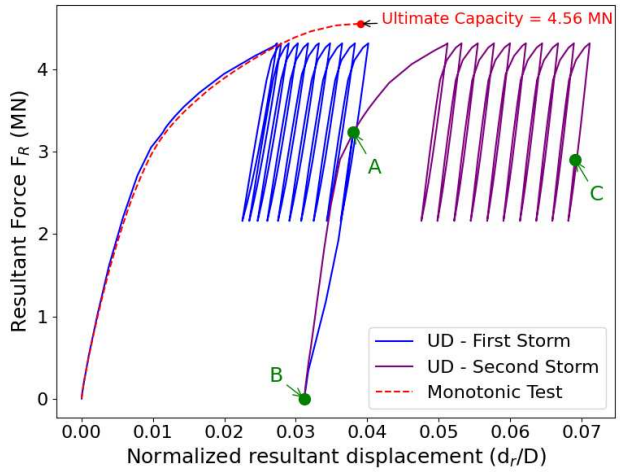

Figure 3 Load-displacement response at pile LRP in monotonic and cyclic unidirectional (UD_0) tests.

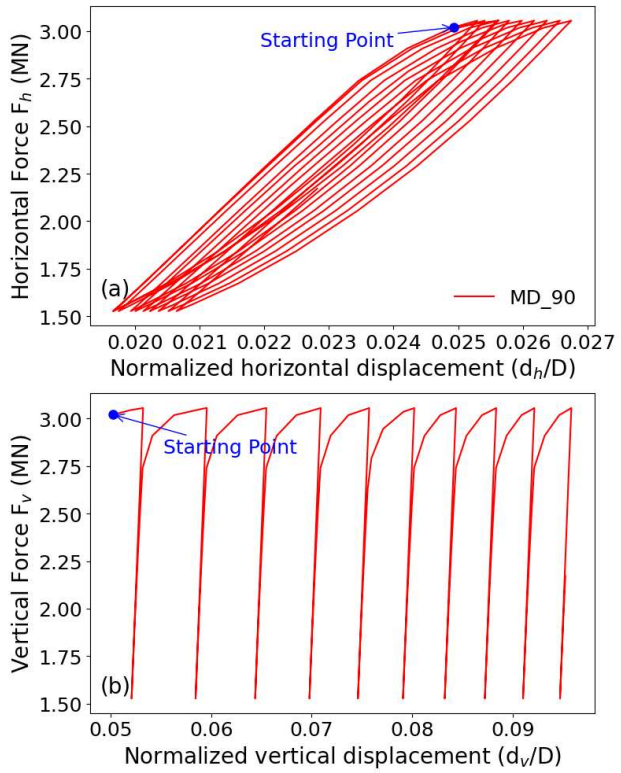

Figure 4 Load-displacement responses of multidirectional test MD_90, α = 90°, for the second storm phase. (a) Horizontal load-displacement response (b) Vertical load-displacement response. (different x-axis)

Further analysis of the observed rates of displacement and behaviour within the soil mass as a function of change in load path direction is presented in Section 3.3.

To quantify the impact of storm directionality on displacement, a multidirectional factor is defined, given by the maximum displacement of each test at cycle 20, normalised by the resultant maximum displacement of the unidirectional test (UD_0) at cycle 20 (Figure 6). Tests with minimal directional change (MD_30 at 30° and MD_45 at 45°) show only a minor increase, less than 10%, in accumulated displacement at cycle 20. In contrast, tests with larger directional deviations (MD_90 and MD_180 at 90° and 180°) exhibit a significant increase of approximately 30-40% in accumulated displacement. Analyzing the horizontal and vertical components of the multidirectionality factor (Figure 6) shows that the effect of multidirectional loading on the accumulated horizontal displacement is minor (<5%), whereas the vertical displacement of the anchor pile is highly sensitive to load direction, changing by up to 40% as α varies from 0 to 180°.

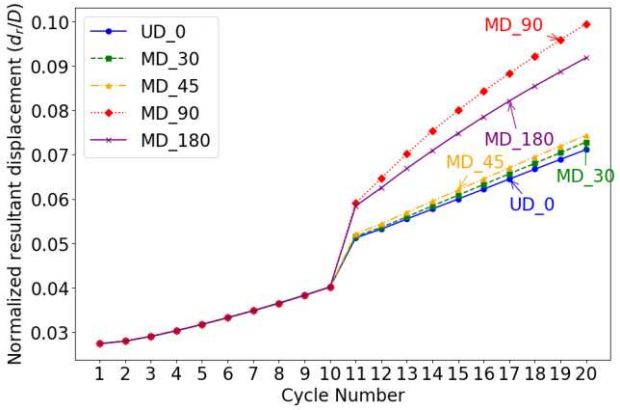

Figure 5 Evolution of normalized resultant displacement (d_r/D) for each loading configuration.

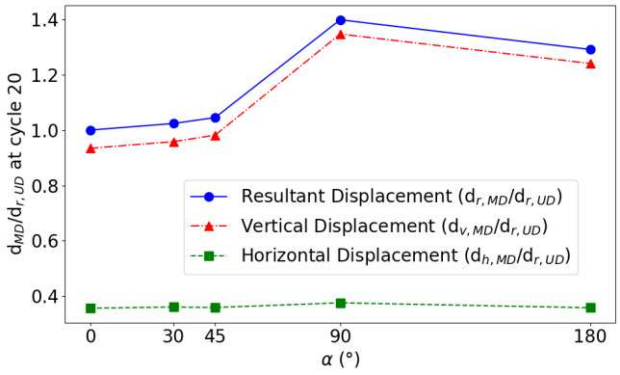

Figure 6 Multidirectionality factor at the end of cycling (cycle 20) for total ($d_{r,MD}/d_{r,UD}$), vertical ($d_{v,MD}/d_{r,UD}$) and horizontal ($d_{h,MD}/d_{r,UD}$) displacements as a function of the change in loading direction angle (α°).

These findings highlight the importance of considering vertical ratcheting effects when evaluating anchor pile stability under multidirectional cyclic loads. A larger load direction variation in the horizontal plane raises the vertical pile displacement, as explored below.

3.3 Effect on void ratio and stress paths

Variations in void ratio and stress condition around the pile are influenced by the changing load direction. Figure 7 shows contours of void ratio at depth 0.5 m below the mudline, indicating the areas of influence around the pile following the first and second storm loading packets. After the first packet of cyclic loading, soil loosening is observed, illustrated in *Figure 7a and b.*

Figure 7c-h illustrate the affected zone after the second storm. It is evident that under low variation of load directionality, the region of loosened soil is limited to the front of the pile, while under high variations in directionality, a larger area around the anchor is loosened.

However, even though test MD_180 involves a equal numbers of cycles in opposite directions, the zone of loosening is not symetrical. Instead, after both packets of loading, there is greater loosening in the direction of the first packet (Figure 7g), and this loosened zone extends to a greater depth (Figure 7h).

Figure 8 shows the cartesian stress path in the horizontal (radial) - vertical plane for an element in front of the pile in the direction of the first loading packet. During the first packet of cycles, the vertical stress rises to more than four times the geostatic value, accompanied by high horizontal stresses consistent with passive failure. After unloading at time B the stresses reduce close to the geostatic values, but with additional locked-in vertical stress.

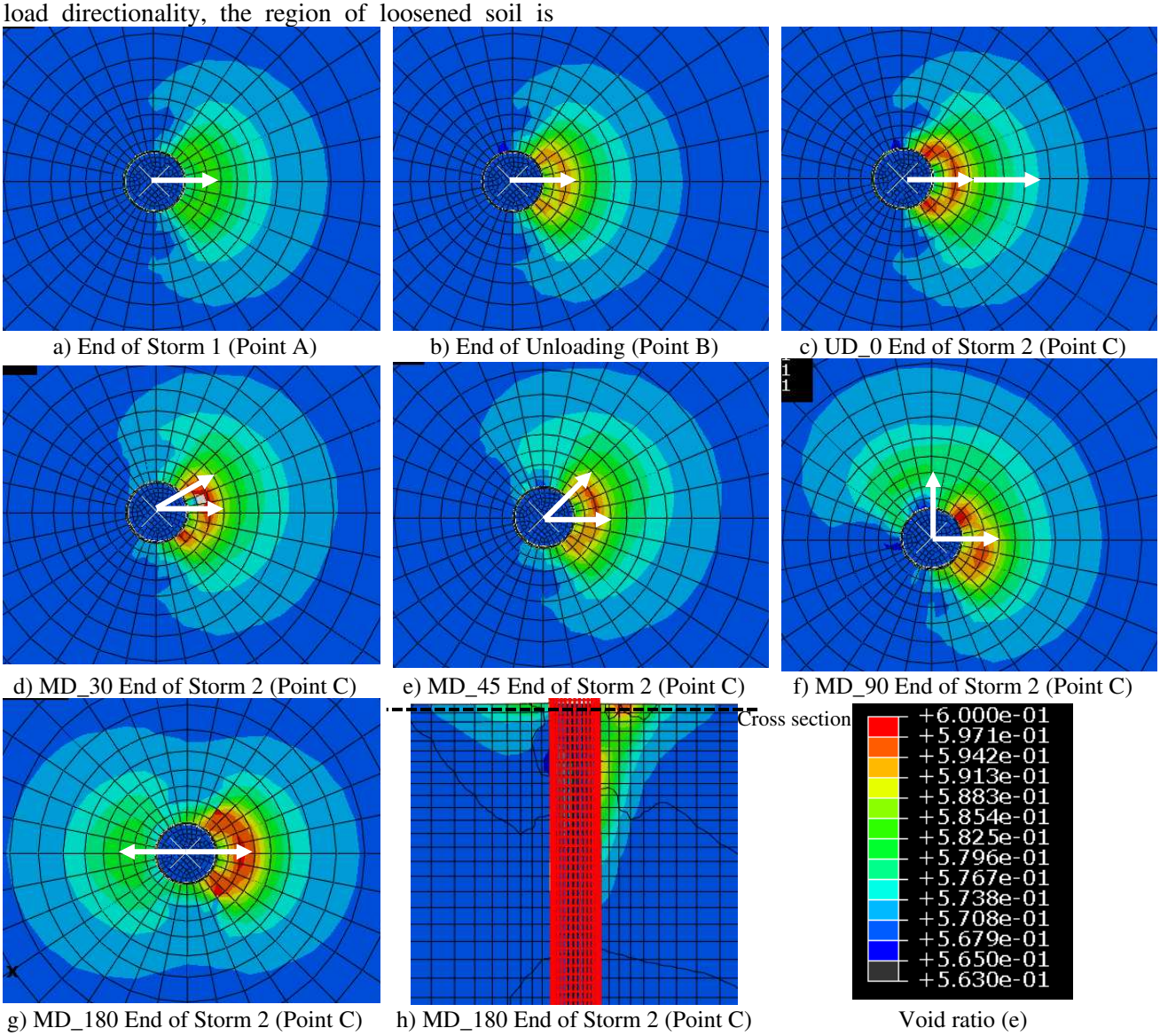

a) End of Storm 1 (Point A)
b) End of Unloading (Point B)
c) UD_0 End of Storm 2 (Point C)
d) MD_30 End of Storm 2 (Point C)
e) MD_45 End of Storm 2 (Point C)
f) MD_90 End of Storm 2 (Point C)
g) MD_180 End of Storm 2 (Point C)
h) MD_180 End of Storm 2 (Point C)
Void ratio (e)

Figure 7 Contour plots of void ratio around the anchor pile at time frames A and B for all tests (a-b). Void ratio at time frame C (end of second storm) for all tests (c-g). Vertical cross section of void ratio at time frame C for test MD_180 (h)

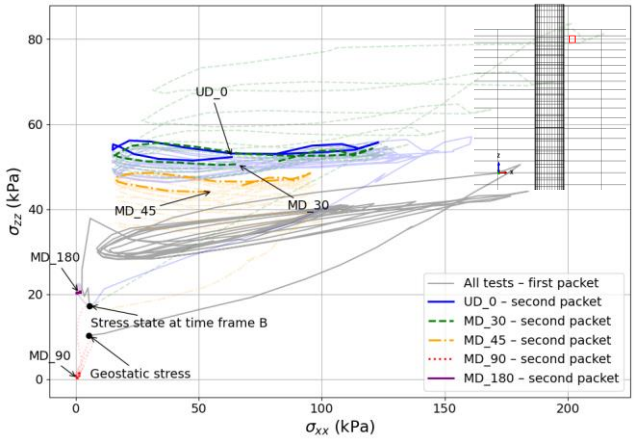

Figure 8 Stress path 0.5 m in front of pile (positive x-direction) at 0.5 m depth. Element location shown in mesh. First packet shown in grey. Second packet coloured with last cycle in bold.

During the second cyclic packet, very different responses are evident. At the start of this packet, the stress rises most significantly in MD_30, but after 20 cycles the cyclic stress path in tests UD_0, MD_30, MD_45 have stabilised to form similar loops. In contrast, the stress in tests MD_90 and MD_180 have fallen to low and stable values, with minimal variation within each cycle.

These very different stress paths, when integrated around and along the pile shaft, lead to variations in the stiffness and capacity of the axial shaft response, explain the variations in axial ratcheting behaviour.

4 CONCLUSIONS

The effect of changing load path direction on the cyclic drained response of a shared pile anchor under inclined uplift loading was investigated using 3D finite element analysis.

The results indicate that the angular variation in the plane of the net force direction applied to the anchor is critical in determining the shared pile behaviour. For low variation in storm directionalities (0-45˚), a minimal increase in ratcheting of around 10% compared to repeated storms in the same direction (i.e. unidirectional) was observed. However, in cases where the loading direction altered significantly between storm packets (i.e. a high inter-storm multidirectionality), ratcheting increased up to 40% above that of the unidirectional case. Nearly all the ratcheting occurred in the vertical direction, signifying that interface stress changes are significantly influenced by load directionality, particularly in the case of steeply inclined loads considered in this study.

The differences in anchor response are linked to distinct cyclic stress paths and void ratio changes around the pile. Changes in loading direction are shown to create very large differences in voids ratio change and stress path around the pile, explaining the contrasting ratcheting behaviour for each case.

This preliminary study into the effects of storm directionality on the cyclic response of an anchor pile signifies the importance of considering load directionality arising from weather patterns for safe design of shared floating wind turbine anchors.

AUTHOR CONTRIBUTION STATEMENT

First Author: Data curation, Formal Analysis, Writing- Original draft, Software, Visualisation. **Other Authors**: Conceptualization, Methodology, Supervision, Writing- Reviewing and Editing.

REFERENCES

Cerfontaine, B., White, D., Kwa, K., Gourvenec, S., Knappett, J., Brown, M., 2023. Anchor geotechnics for floating offshore wind: Current technologies and future innovations. Ocean Eng. 279, 114327. https://doi.org/10.1016/j.oceaneng.2023.114327

Chow, S.H., Roy, A., Herduin, M., Heins, E., King, L., Bienen, B., O'Loughlin, C., Gaudin, C., Cassidy, M., 2019. Characterisation of uwa superfine silica sand.

Coughlan, K., 2024. Mooring systems for floating offshore wind: Mooring design, biocolonisation, and shared anchors.

Dassault Systèmes, 2023. Abaqus/standard user manual.

Equinor, 2023. Hywind tampen. Https://www.Equinor.Com/energy/hywind-tampen.

Fontana, C.M., Hallowell, S.T., Arwade, S.R., DeGroot, D.J., Landon, M.E., Aubeny, C.P., Diaz, B., Myers, A.T., Ozmutlu, S., 2018. Multiline anchor force dynamics in floating offshore wind turbines. Wind Energy 21 (11), 1177-1190. https://doi.org/10.1002/we.2222

Herduin, M., 2019. Multi-directional loading on shared anchors for offshore renewable energy: Definition and preliminary investigation into soil behaviour and anchor performance.

LeBlanc, C., Houlsby, G.T., Byrne, B.W., 2010. Response of stiff piles in sand to long-term cyclic lateral loading. Géotechnique 60 (2), 79-90. https://doi.org/10.1680/geot.7.00196

Niemunis, A., Herle, I., 1997. Hypoplastic model for cohesionless soils with elastic strain range. Mechanics of Cohesive-frictional Materials 2 (4), 279-299. https://doi.org/10.1002/(sici)1099-1484(199710)

Pillai, A.C., Gordelier, T.J., Thies, P.R., Cuthill, D., Johanning, L., 2022. Anchor loads for shallow water mooring of a 15 mw floating wind turbine—part ii: Synthetic and novel mooring systems. Ocean Eng. 266. https://doi.org/10.1016/j.oceaneng.2022.112619

Richards, I.A., Byrne, B.W., Houlsby, G.T., 2020. Monopile rotation under complex cyclic lateral loading in sand. Géotechnique 70 (10), 916-930. https://doi.org/10.1680/jgeot.18.P.302

Sheil, B.B., McCabe, B.A., 2017. Biaxial loading of offshore monopiles: Numerical modeling. Int. J. Géomech. 17 (2), 04016050. https://doi.org/10.1061/(asce)gm.1943-5622.0000709

Staubach, P., Machaček, J., Wichtmann, T., 2021. Large-deformation analysis of pile installation with subsequent lateral loading: Sanisand vs. Hypoplasticity. Soil Dyn. Earthq. Eng. 151, 106964. https://doi.org/10.1016/j.soildyn.2021.106964